



Length reduction kinetics of multiwalled carbon nanotubes correlated to planetary ball mill impact energy

Mason A. Rhue, Mahmoud Zaqout, Caleb Bavlnka, Steven Crossley (1), and Brian P. Grady (1)

School of Sustainable Chemical, Biological & Materials Engineering, University of Oklahoma, Norman, OK, USA

ABSTRACT

Four commercial multiwalled carbon nanotubes with distinct lengths and diameters were subject to planetary ball milling to induce length reduction. The Burgio-Rojac energy model was employed to calculate the single impact energy and cumulative energy dissipated to the carbon nanotubes during milling. The ratio of sample mass to bead mass and the nanotube bulk density did not affect length reduction during grinding. The minimum impact energy barrier for carbon nanotube length reduction appeared directly proportional to nanotube diameter for parallel wall morphologies, although a nanotube sample with a cup-stacked wall morphology showed a much lower energy barrier. A normalized exponential equation relating carbon nanotube length and cumulative impact energy collapsed all data to a single exponential master curve described by the same scaling parameters, namely a pre-exponential term that includes the initial nanotube length and a scaling energy in the exponent.

ARTICLE HISTORY

Received 23 June 2023 Accepted 12 September 2023

KEYWORDS

Carbon nanotubes; ball milling; Burgio-Rojac model

1. Introduction

Carbon nanotubes show great evidence as additives in polymer composites to boost mechanical, [1,2] electrical, [3-6] and thermal properties.^[7-9] Regarding electrical properties, compared to similar carbon nanomaterials like carbon fiber and carbon black, carbon nanotubes produce nanocomposites with significantly lower percolation thresholds for achieving these improved properties.^[10,11] However, the cost of carbon nanotubes currently limits their commercial viability as higher loading percentages of more affordable carbon materials often result in lower overall composite costs. The high cost of carbon nanotube production is generally attributed to low industrial yields and purification processes needed after the growth on catalyst materials. Current strategies to lower the cost of carbon nanotubes include increasing yield by increasing nanotube length upwards of hundreds of microns to millimeters, which is possible for nanotubes grown on flat surfaces. [12,13] High yield processes can potentially eliminate the need to separate carbon nanotube product from catalyst and support material, leading to lower overall manufacturing cost. However, long nanotubes from high yield processes introduce a variety of processing issues like high melt viscosity when compounded into a polymer. If very long nanotubes were used, then during a mixing process in a twin-screw extruder significant polymer molecular weight degradation would be expected due to the high shear forces caused by long nanotubes. Hence, the length of the tubes would almost certainly need to be reduced prior to compounding. The purpose of this work is to examine the

length reduction of carbon nanotubes *via* ball milling to better understand how nanotube diameter, length, and packing density affect length reduction kinetics.

Attempts have been made previously to model the kinetics of carbon nanotube length reduction based on parameters of the breaking process. Studies on carbon nanotube length reduction by sonication compare the different possible mechanisms of breakage such as tensile, [14,15] compression, [16] and buckling. [17] The kinetic behavior of length reduction by sonication consistently shows a power law relationship between cumulative sonication energy and resulting carbon nanotube length. [14,15,17,18] These data indicate that a terminal length can eventually be reached, and of course the power law fit was not extended to this limit. [15] However, the dependence of length reduction on energy varies in different studies and seems to vary for different nanotube morphologies (i.e. parallel wall, cup-stacked, bamboo-shaped, etc.). [19] Also, implementing sonication on an industrial scale would prove difficult as it would require further separation of the carbon nanotubes from the solvent.

Ball milling is a commonly used industrial process to separate carbon nanotubes from catalyst and support material, [20] functionalize carbon nanotube surfaces and ends, [21-23] improve carbon nanotube dispersion in metal [24-30]/metal-oxide [31-33] and polymer [34-37] nanocomposites, and reduce carbon nanotube length. [38-40] Ball milling as a means of length reduction is particularly enticing due to its relative simplicity, low cost, and capacity for optimization on an industrial scale. Attempts to correlate carbon

Table 1. Initial characteristics of commercial MWCNTs. Errors represent one standard deviation determined by fitting the distribution to a normal distribution.

MWCNT	Length (nm)	x ₁₀ -x ₅₀ -x ₉₀ (nm)	Diameter (nm)	Number of Walls	Bulk Density ^a (g/cm ³)
NC7000s	1327	511-1221-2307	10.8 ± 2.6	9.3 ± 1.1	0.077
C150Ps	810	305-717-1296	13.8 ± 4.7	13.1 ± 1.5	0.010
SMW200s	2062	576-1721-4027	10.6 ± 3.7	9.6 ± 1.2	0.045
Cheap Tubes	1089	390-890-1940	19.2 ± 4.2	16.5 ± 1.5	0.173

^aBulk densities were measured using the method given by Zapata et al.^[51]

nanotube length reduction to ball milling parameters like milling time have been made previously. $^{[41]}$ However, these correlating equations cannot be applied to other systems due to the use of system-specific parameters. Further, many ball milling studies only model length reduction based on milling time without sufficient detail to other important parameters like rotational speeds, grinding media size and material, etc., making it difficult, if not impossible, to extend these results to different carbon nanotubes or different milling conditions. Correlations of carbon nanotube length reduction to ball milling parameters must encompass all these details.

Burgio et al.^[42,43] derived an expression that models the impact energy of planetary ball milling for use in Fe-Zr system mechanical alloying. Further studies adding detail to the mathematical understanding of planetary ball milling validated this energy model based on power measurements during mechanical alloying [44,45] and made corrections to the impact energy expression considering factors like collision elasticity^[46] and grinding media hindering. This energy model was particularly useful in correlating the cumulative energy of milling to phase changes in the Pd-Si, [47] Ti-Al, [48] and Mo-Si^[49] alloy systems. Kozma et al.^[50] were the first and only group to our knowledge to apply this energy model to planetary ball milling of carbon nanotubes. They found that, for a single type of carbon nanotube, an impact energy barrier exists at 35 mJ for which the defect density, measured by Raman spectroscopy, increases substantially. Like the sonication studies, an apparent terminal length was found at high milling times where little to no further length reduction occurred.

In this study, four commercial carbon nanotube samples with distinct lengths and diameters were subjected to planetary ball milling to reduce their length. The Burgio-Rojac model for planetary ball milling was used to determine the single impact and cumulative energies of milling. Effects of milling time, rotational speed, sample mass, and initial powder morphology on the length reduction of carbon nanotubes were investigated. The minimum energy was identified for each nanotube and was seen to correlate to physical characteristics of the nanotube. An exponential function correlating the cumulative energy of milling to the length reduction was derived. Normalization of the length data enabled the data to be fitted by one master curve for all four nanotube samples, and a best fit scaling energy parameter was identified. A comparison between the breaking mechanism and power law kinetic behavior of ball milling and sonication as the method of carbon nanotube length reduction is also given.

2. Experimental

2.1. Materials

Four commercial multi-walled carbon nanotubes were used in this study: Nanocyl TM NC7000 (Nanocyl SA, Sambreville, Belgium), Baytubes[®] C150P (Bayer MaterialScience AG, Leverkusen, SMW200 Germany), Nanotechnologies, Norman, OK), and Cheap Tubes Short Multi Walled Carbon Nanotubes (Cheap Tubes Inc., Grafton, Vermont). Relevant initial characteristics of these MWCNTs are given in Table 1; these Baytubes® had a very low density relative to other samples with the same tradename. Figure 1 displays the distribution of diameters for each commercial MWCNT measured by TEM, and the shape of the distributions are consistent with those found elsewhere. [41] Figure 2 shows micrographs of the as-received tubes.

2.2. Ball milling

Carbon nanotube length reduction was carried out in a Retsch PM100 Planetary Ball Mill. An 80 mL stainless steel grinding jar (6 cm diameter \times 3.6 cm height) was used with 25 10-mm stainless steel grinding balls. Milling parameters (rotational speed and milling time) and sample parameters (sample mass, initial morphology, and carbon nanotube length/diameter) were varied to evaluate their effects on carbon nanotube length reduction. Rotational speed varied between 100 rpm and 600 rpm at constant milling times of 30 min. Milling time varied between 5 and 60 min at the constant rotational speed of 300 rpm. Additional trials up to 90 min were obtained when necessary to ensure the terminal length had been reached. For the NC7000s trials, sample masses of 2 g, 1.2 g, and 0.4 g were used in the milling process to determine sample mass effects. NC7000s with different initial bulk densities were obtained by dispersing the pure NC7000s in water and allowing the water to evaporate, leaving the powder in a more aggregated state. The resulting bulk density was almost double that of the initial powder.

2.3. Electron microscopy

Carbon nanotubes were characterized by both scanning (SEM) and transmission (TEM) electron microscopy. Zeiss Neon 40EsB and Thermofisher Quattro S SEMs were used to image carbon nanotube samples for length measurements. By the method of Krause et al. [52], raw commercial and milled carbon nanotube powders were dispersed in a solvent via an ultrasonic bath at a concentration of 0.1 g/L to

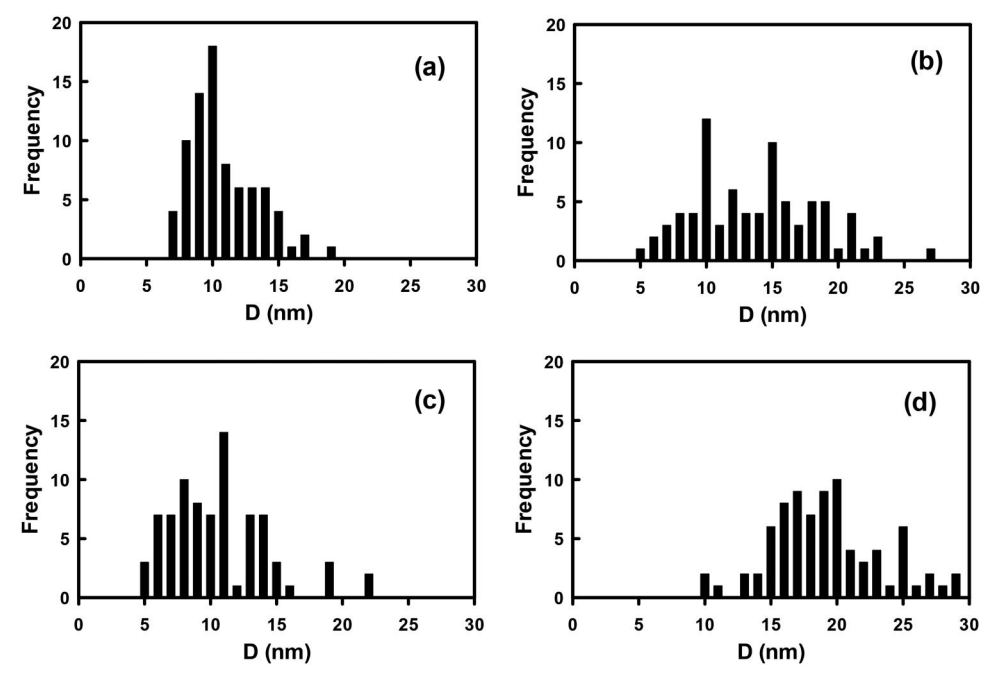


Figure 1. Diameter histograms of (a) NC7000s, (b) C150Ps, (c) SMW200s, and (d) Cheap Tubes.

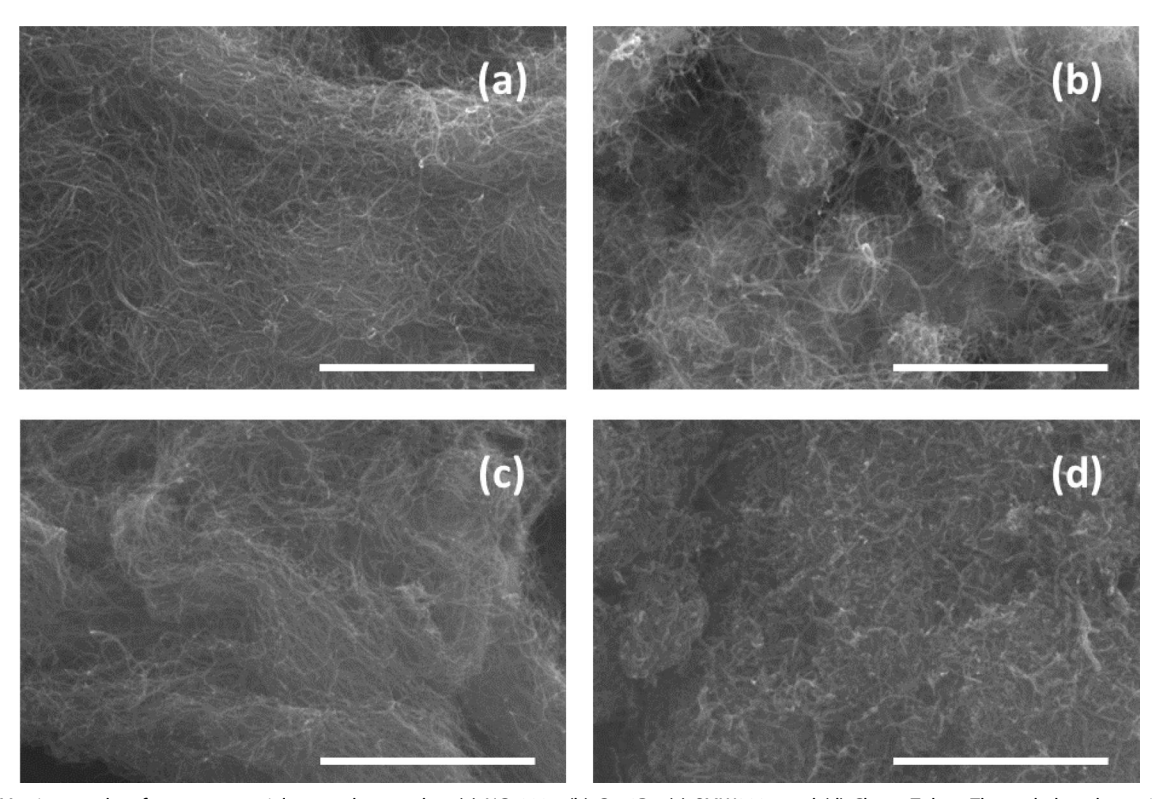


Figure 2. SEM micrographs of raw commercial nanotube powders (a) NC7000s, (b) C150Ps, (c) SMW200s, and (d) Cheap Tubes. The scale bar shown in each image is $2 \mu m$.

promote individualization of the nanotubes. Dispersing solvents for each nanotube sample were chosen by trial and error based on how well the nanotube phase dispersed during sonication and stayed dispersed after sonication. Chloroform was used as the dispersing solvent for NC7000s, C150Ps, and SMW200s, and isopropanol was used for the Cheap Tubes. A drop of this dispersion was transferred to

a polished silicon wafer for imaging. Fiji (ImageJ) image processing software was used to manually measure the length of carbon nanotubes captured in the SEM micrographs. Micrographs containing long carbon nanotubes were stitched together when necessary to ensure the full nanotube length could be measured accurately. The average length for a nanotube sample was taken as an average

of at least 100 measurements. Length distribution parameters x_{10} , x_{50} , and x_{90} representing that 10%, 50%, and 90% of carbon nanotube lengths in the sample fall below the x_{10} , x_{50} , and x_{90} value are presented in Table 1.

Diameters and number of walls of the carbon nanotubes were determined by micrographs taken on a JEOL 2010 F TEM. Nanotube powders were suspended in ethanol to promote individualization of the nanotubes, and roughly $4\,\mu\text{L}$ were pipetted onto a 200-mesh lacey carbon grid from Ted Pella, Inc. The diameters were measured directly while the number of walls, N_w , was calculated by the following

$$N_w = \frac{\left(\frac{D_o - D_i}{2}\right)}{0.34 \ nm} \tag{1}$$

where D_o and D_i are the outer and inner diameters of the nanotube and 0.34 nm is the van der Waals atomic diameter of carbon and consequently the width of a single wall. [53] Fiji (ImageJ) was used to measure the diameters of carbon nanotube samples. The average diameters given in Table 1 are an average of at least 80 measurements.

2.4. Raman spectroscopy

Raman spectra of carbon nanotube samples were captured using a Renishaw inViaTM confocal Raman microscope and spectrometer. A 532 nm laser (45 W) was used at five percent laser power. Additionally, a 2400 l/mm diffraction grating was used. Spectrum acquisition conditions used were five seconds of exposure time and three accumulations. The Raman peaks of interest for this study were the G band centered around 1565-1585 cm⁻¹ and the D band centered around 1330-1350 cm⁻¹. The G band is indicative of graphitic sp² hybridization, while the D band is related to defects in graphitic structures.^[54] The ratio of the D band to G band peak areas, notated as I_D/I_G , was used as a measure of the defect density in the carbon nanotube sample as done previously. [50] I_D/I_G values approaching infinity indicate a high defect density, while I_D/I_G values approaching zero indicate a low defect density. To calculate the I_D/I_G values, peak areas were obtained from the integrated WiRETM software after performing baseline subtraction, normalization, and curve fitting on each individual spectrum.

2.5. Energy calculations

The Burgio-Rojac model was used to evaluate the energy input during planetary ball milling. [43] The impact energy for one impact, E_b , is given by

$$E_{b} = \frac{1}{2} \varphi_{b} \left(\rho_{b} \frac{\pi d_{b}^{3}}{6} \right) \omega_{p}^{2} \left[\left(\frac{\omega_{v}}{\omega_{p}} \right)^{2} \left(\frac{d_{v} - d_{b}}{2} \right)^{2} \left(1 - 2 \frac{\omega_{v}}{\omega_{p}} \right) - 2r_{p} \left(\frac{\omega_{v}}{\omega_{p}} \right) \left(\frac{d_{v} - d_{b}}{2} \right) - \left(\frac{\omega_{v}}{\omega_{p}} \right)^{2} \left(\frac{d_{v} - d_{p}}{2} \right)^{2} \right]$$
(2)

where φ_b is the obstruction factor, ρ_b is the density of the grinding balls, ω_p and ω_v are the rotational speeds (rad/s) of the sun wheel and grinding jar, respectively, d_v and d_b are

the diameters of the grinding jar and grinding balls, respectively, and r_p is the radius of the sun wheel. The speed ratio, ω_{ν}/ω_{p} , provided by Retsch for the PM100 mill is -2. The velocity expression in the impact energy equation derives from the difference between the launched velocity of a grinding ball due to the rotation of the sun wheel/grinding jar and the velocity after an impact. The impact energy thus corresponds to the energy dissipation upon impact. While Equation (2) assumes a perfectly inelastic collision, corrections of collision elasticity can be made by multiplying the impact energy by a parameter K_a with a value between 0 and 1 indicating a perfectly elastic ($K_a = 0$) or perfectly inelastic ($K_a = 1$). However, this correction was not made in this study as free fall experiments with coated grinding balls have shown changes in collision elasticity to be inconsequential in the early stages of milling. [46]

The obstruction factor is dependent on the degree of filling in the jar and is calculated by the following

$$\varphi_h = 1 - n_v^{\varepsilon} \tag{3}$$

where n_v is the fraction of filled space by grinding balls in the grinding jar and ε is a parameter dependent on the geometry of the mill.

$$n_{\nu} = \frac{N_b}{N_{h,\nu}} \tag{4}$$

$$N_{b,\nu} = \frac{\pi d_{\nu}^2 h_{\nu}}{4d_{b}^3} \tag{5}$$

$$n_s = \frac{N_b}{N_{b,s}} \tag{6}$$

$$N_{b,s} = \frac{\pi (d_v - d_b) h_v}{3d_v^2} \tag{7}$$

 N_b is the number of grinding balls in the grinding jar and h_v is the height of the grinding jar. $N_{b,v}$ is the number of grinding balls in a cubic arrangement that would fill the grinding jar and $N_{b,s}$ is the number of grinding balls in a cubic arrangement that would cover one third of the inner surface area of the grinding jar. The value of parameter ε is found by the following

$$0.95 = 1 - \left(\frac{N_{b,s}}{N_{b,v}}\right)^{\varepsilon} \tag{8}$$

and for this study is calculated to be 1.7764, very similar to the value found by Bugio et al. [43] for balls of 10 mm diameter.

The cumulative energy of milling, E_{cum} , is the product of the single impact energy and the number of impacts over the milling period and is given by the following

$$E_{cum} = E_b \nu_t t \tag{9}$$

where v_t is the impact frequency and t is the milling time. The impact frequency is calculated as described by Magini et al.^[45]

$$v_t = N_b K(\omega_p - \omega_v) \tag{10}$$

where K, is an instrument parameter dependent on the geometry of the mill. The value of instrument parameter K is generally around ~ 1 and has been shown to be 1.5 for grinding balls 8-10 mm in diameter.

3. Results and discussion

3.1. Minimum impact energy

The length reduction of the four commercial nanotube samples with respect to increasing rotational speed, and consequently increasing impact energy, at constant milling time is shown in Figure 3. The length reduction behavior of NC7000s shows no significant differences among different sample masses and different initial bulk densities. The invariance of length differences with powder mass is not surprising. Magini et al. [46] stated that milling powder forms a coating on all surfaces of grinding balls and walls during the early stages of milling, and collisions between these balls entrap all the powder within the collision radius. Varying the sample mass effectively changes the coating thickness of the surfaces inside the grinding jar, and the results show that the breaking efficiency of these impacts is sufficient to break the nanotubes trapped in the collisions for even the thickest coating in this study. Another critical assumption is that the entire powder sample is coating a surface, and there

is no unfixed powder in the jar during milling. Deviations from this assumption would likely result in less nanotube breakage as this free moving powder does not participate in the collisions. However, visual observations of the nanotube powder in the grinding jar after milling validates the assumption that no free moving powder exists under the conditions used in our experiments.

The length reduction behavior of NC7000s, SMW200s, and C150Ps are all very similar. A distinct horizontal step at low impact energies is followed by an exponential-type length decrease. Clearly, these nanotubes possess a minimum impact energy for which under that energy, no significant length reduction has occurred, and above that impact energy, fracture does occur. For the NC7000s and SMW200s, the minimum impact energy appears to be 10 mJ, while the minimum impact energy for the C150Ps is 15 mJ. This result suggests that the minimum energy for breakage of a carbon nanotube is dependent on the diameter or number of walls. The NC7000s and SMW200s both have very similar average diameters and number of walls and show similar minimum impact energies, while the C150Ps have a larger diameter and number of walls and have a larger minimum impact energy. This increase is likely consistent with the findings of Kozma et al. [50], who found that nanotubes of 30 nm in diameter possess a minimum energy

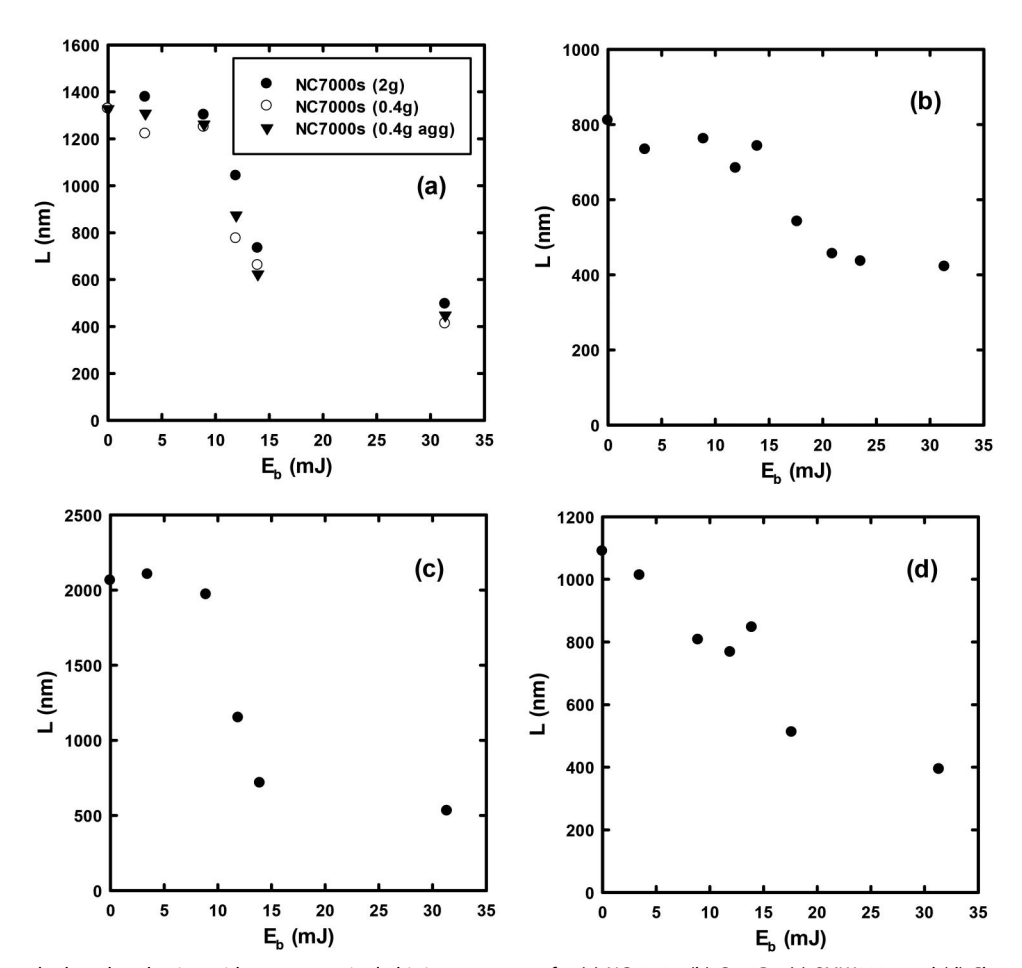


Figure 3. Carbon nanotube length reduction with respect to single hit impact energy for (a) NC7000s, (b) C150Ps, (c) SMW200s, and (d) Cheap Tubes.

of 35 mJ, although the number of walls is not given. TEM micrographs confirm that ball milling did not reduce the carbon nanotube diameter for any of the nanotubes. This result is consistent with most studies, [41] but others have shown high energy ball milling (HEBM) can result in partial wall damage or complete destruction of nanotubes.^[55]

The length reduction behavior of the Cheap Tubes has a different form than the other three nanotubes. No distinct horizontal step occurs at low impact energies, and the length reduction up to 30 mJ is nearly linear. Figure 3d shows the Cheap Tubes possess a minimum energy below 3.5 mJ, which is the lowest impact energy we studied. This result is likely explained by TEM micrograph analysis of the virgin tubes in which wall damage and alternative nanotube morphologies were seen. Based on TEM images, Cheap Tubes possess a high concentration of wall damage and dislocations compared to the other three nanotube samples. The presence of wall damage likely weakens the structural integrity of the nanotubes, leading to a reduced minimum impact energy. These defects could be a byproduct of the industrial synthesis process or of milling performed by the manufacturer to separate the nanotubes from the catalyst and support materials. Also, as shown in Figure 4, many nanotubes within the TEM micrographs appeared to have a cupstacked or bamboo-like morphology. These layers could be more easily sheared apart due to open ends on the nanotube surface, also leading to lower ball impact energies required to fracture the nanotube. Linear length reduction with respect to increasing impact energy as found with Cheap Tubes was consistent with the findings of Kozma et al. [50] However, they identified the minimum energy with Raman spectroscopy rather than with length measurements. The initial carbon nanotube product possessed a low concentration of defects, and there was a marked increase in I_D/I_G at 35 mJ, indicating an increase in sp³ hybridized carbons. This observation was used as justification for identifying the minimum energy despite the length having already been reduced by nearly 50%.

Raman spectra and I_D/I_G values corresponding to the 0.4 g milled NC7000s samples in Figure 3a are given in Figure 5. Variations in the peak ratio have no correlation

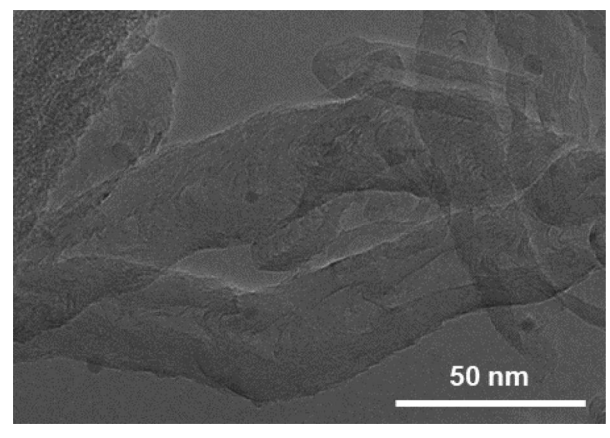


Figure 4. Enhanced and cropped HRTEM micrograph of Cheap Tubes with apparent cup-stacked wall morphologies.

with the average nanotube length. For this peak ratio to be a proper measure of minimum impact energy determination, it would be expected that a distinct increase in I_D/I_G occurs when the average length of the NC7000s reduces significantly. Similar results were found for the other three commercial nanotubes studied. Raman spectra and I_D/I_G values for C150Ps, SMW200s, and Cheap Tubes milled at different impact energies can be found in Figures S5-S7 in the Supplemental Information section. A primary concern of the authors was that nanotube healing may have occurred after ball milling of the nanotubes and before Raman spectra acquisition (ball milling and spectra acquisition occurred months apart). To explore the possible effect of nanotube healing, Raman spectra of freshly milled NC7000s under the same conditions as stated for Figure 3a were acquired, and no appreciable changes in the spectra or peak ratios were observed.

It is assumed that defect-dense nanotube ends account for a large portion of the D band detected by Raman spectroscopy. Assuming the defect-dense length of a nanotube accounts for 5 nm on each nanotube end, then for unmilled NC7000s (\sim 1330 nm) approximately 0.8% of the nanotube length is defect-dense. For NC7000s milled to their terminal length (~410 nm), the defect-dense length fraction increases to approximately 2.4%. A marginal increase in defect-dense length is not likely to produce notable changes in the Raman shift, so the peak ratio values obtained in this study are likely within the margin of error. However, we recognize that nanotube samples may experience slight wall damage and amorphization, contributing further to D band amplification. Thus, we believe that length measurements should be the primary method of identifying the minimum impact energy since $E_{b,\,\mathrm{min}}$ has been defined as the energy required to fracture a nanotube into shorter segments.

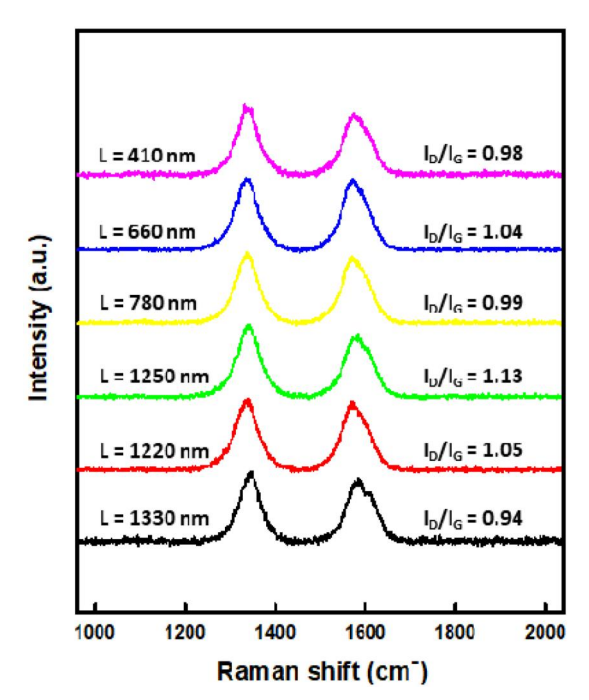


Figure 5. Raman spectra (Background subtracted and normalized) and I_D/I_G values associated with the 0.4 g milled NC7000s samples in Figure 3a.

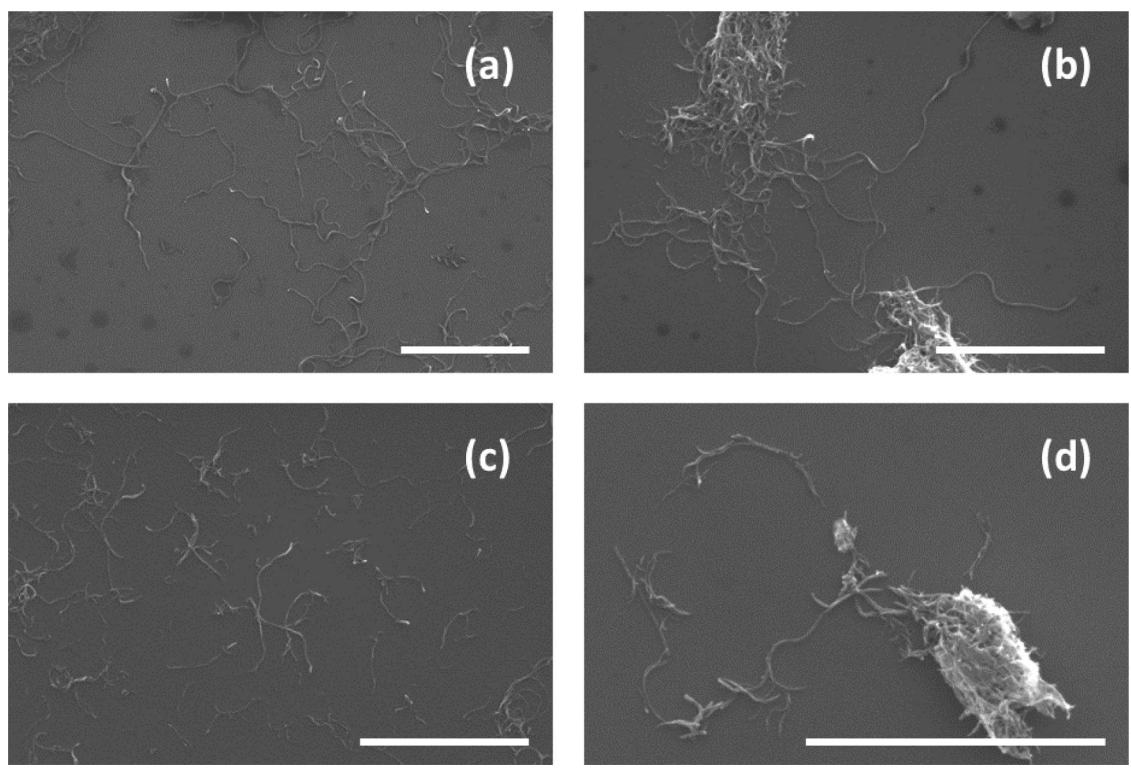


Figure 6. SEM micrographs of (a) pure NC7000s and milling times of (b) 10 min, (c) 20 min, and (d) 30 min. The scale bar shown in each image is 2 µm.

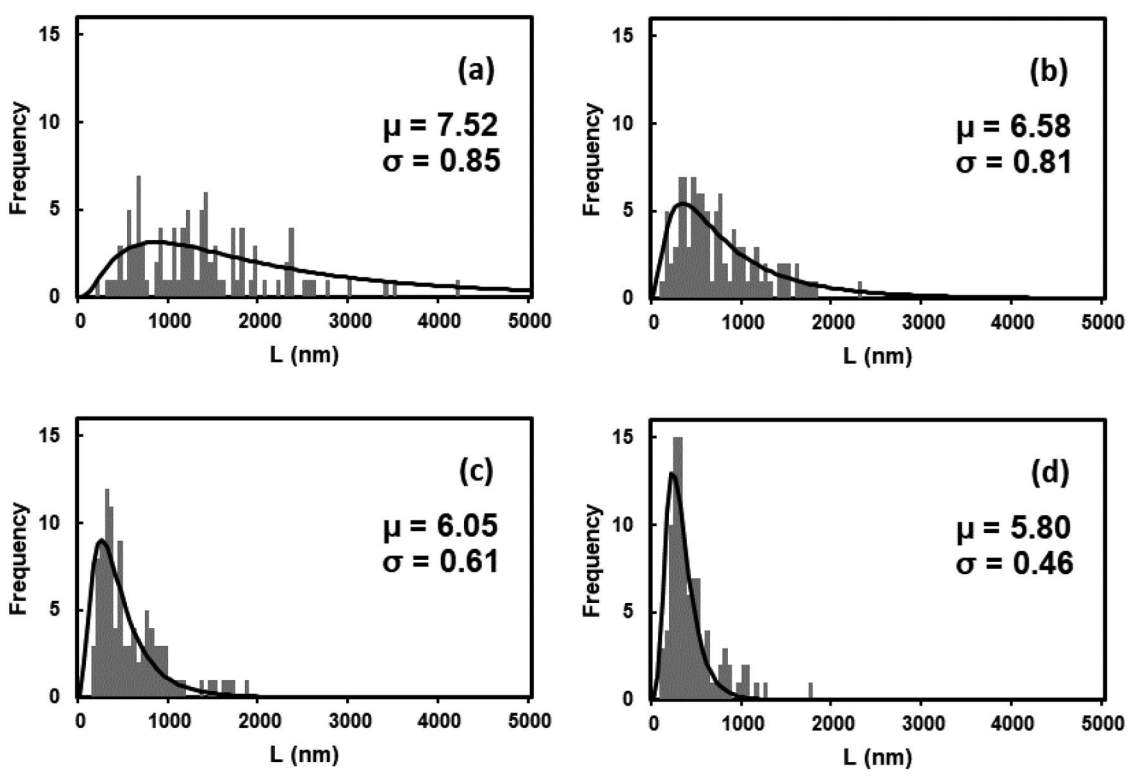


Figure 7. Length distributions for (a) pure NC7000s and 0.4 g trial milling times (and cumulative energies) of (b) 10 min (67 kJ), (c) 20 min (133 kJ), and (d) 30 min (200 kJ). the data appears to best fit a log-normal distribution and parameters μ and σ are given.

3.2. Cumulative energy of milling

To obtain a range of cumulative energies, the rotational speed of the mill was kept constant at 300 rpm, corresponding to roughly an impact energy of 30 mJ, and the milling

time was increased. The length reduction of NC7000s (0.4 g trials) is evident based on the SEM micrographs given in Figure 6 and the corresponding length distributions, along with log-normal fit and distribution parameters μ and σ ,

given in Figure 7. The unmilled NC7000s are clearly the longest upon visual observation and have the widest distribution of lengths. Nanotubes on the order of 4-5 µm in length span a large portion of the field of view, and in many cases image stitching was necessary to measure full nanotube lengths. At 20 min of milling, all nanotubes appear to be at or below 2 µm, and this observation is reinforced by the length distribution given in Figure 7c. At 30 min of milling, the distribution becomes very narrow and no further significant length reduction was seen. The goodness of the log-normal fit is most evident at higher milling times. Although the fits are not shown here, this same log-normal function type was able to fit the length distribution of all tubes well at higher milling times. Length reduction upon milling of all nanotubes tested in this study follow this same qualitative pattern with time as shown in Figures S1-S4 in the Supplementary Information. The tendency for ball milled carbon nanotubes to converge to a log-normal distribution has been shown previously, [56] but other fits such as the Weibull distribution have been observed.[57]

The length reduction behavior of the four commercial carbon nanotube samples with respect to increasing cumulative energy is shown in Figure 8. The length reduction behavior of NC7000s shows no variance among the different sample masses and initial bulk densities. The appearance of a terminal length around 400 nm is consistent with the results of the curve shown in Figure 3a. Also, the fact that changes in mass do not change the length reduction behavior with respect to cumulative energy validates the use of the cumulative energy expression given in Equation 9 as opposed the mass-averaged cumulative elsewhere.[50,58]

Each carbon nanotube sample undergoes exponential length reduction to a terminal length unique to each nanotube sample. For the NC7000s, C150Ps, and SMW200s, the experimental terminal length is nearly 400 nm, while the Cheap Tubes converge to approximately 250 nm. The shorter terminal length of the Cheap Tubes indicates that cup-stacked wall morphologies may make nanotubes more susceptible to further length reduction to smaller aspect ratios. The terminal length for each nanotube is achieved at

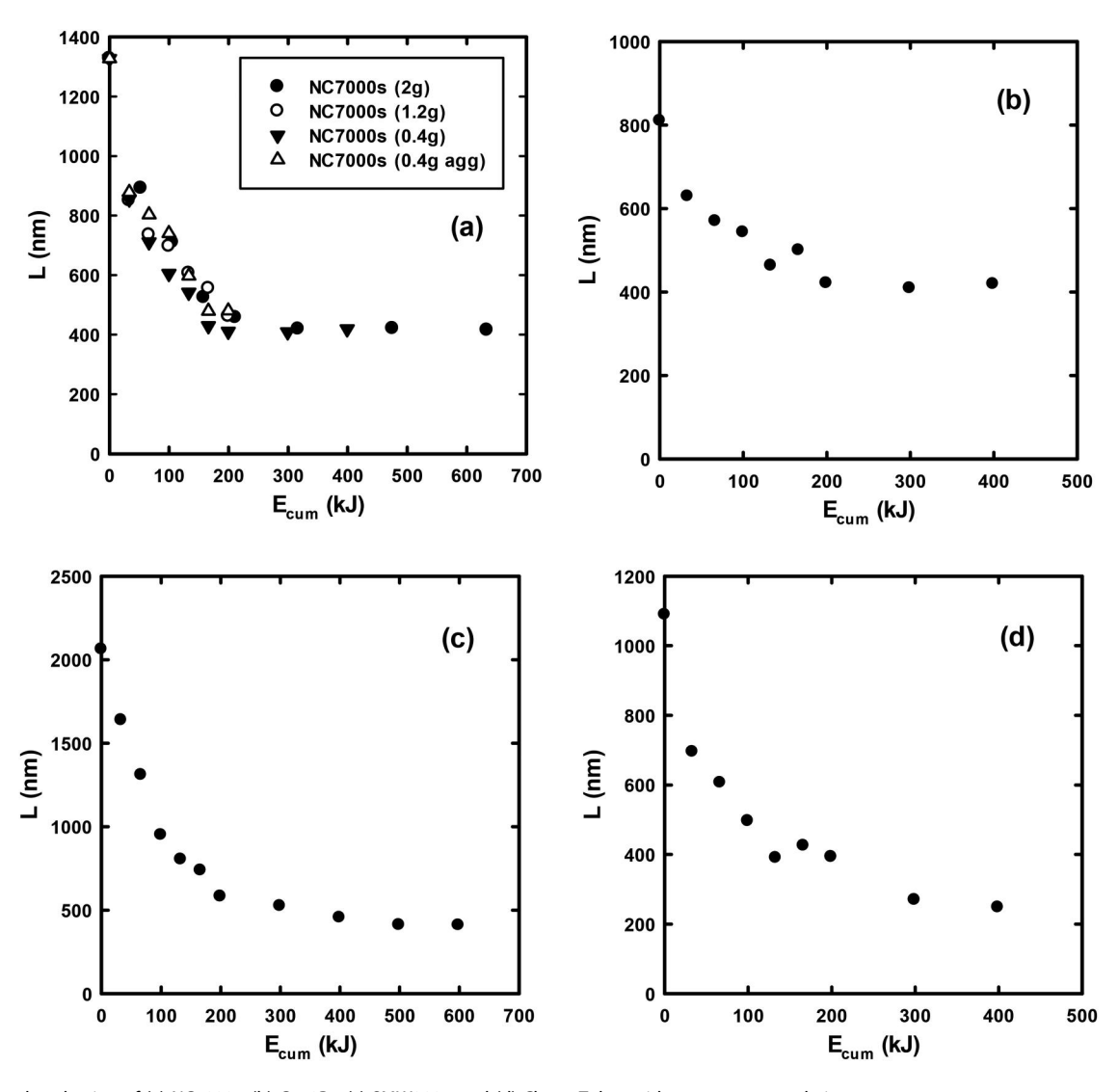


Figure 8. Length reduction of (a) NC7000s, (b) C150Ps, (c) SMW200s, and (d) Cheap Tubes with respect to cumulative energy.

a cumulative energy of 350 kJ. The asymptotic behavior of carbon nanotube length reduction at high cumulative energies is consistent with what has been found in the literature for ball milling, [56] although other high energy ball milling studies have shown carbon nanotubes can be further reduced to nanoparticles and amorphous carbon. [59,60]

3.3. Master curve

An exponential equation relating carbon nanotube length to the cumulative energy of milling was derived as shown

$$L = (L_o - L_f)e^{\frac{-E_{cum}}{E_{scale}}} + L_f \tag{11}$$

where L_o is the initial length of the raw commercial carbon nanotubes, L_f is the terminal length, and E_{scale} is a scaling energy found by nonlinear regression. E_{scale} was selected to have units of kJ to ensure a unitless exponent. The limits were set so that at zero cumulative energy, the function is equivalent to the initial average length of the raw commercial powder, and at sufficiently high cumulative energies, the function converges to the terminal length. Rearrangement of Equation (11) yields a dimensionless length term which we will call the normalized length difference.

$$\frac{L - L_f}{L_o - L_f} = e^{\frac{-E_{cum}}{E_{scale}}} \tag{12}$$

At zero cumulative energy, the normalized length difference is 1, and at sufficiently high cumulative energies, the normalized length difference converges to 0.

Length reduction data given in Figure 8 for increasing cumulative energy was converted to the normalized length difference, and the four curves representing each commercial nanotube collapsed to a single master curve in Figure 9. The fitted scaling energy parameter, E_{scale} , was found to be 83.7 ± 2.8 kJ. Visual observation of Figure 9 shows good agreement among the four commercial nanotube length

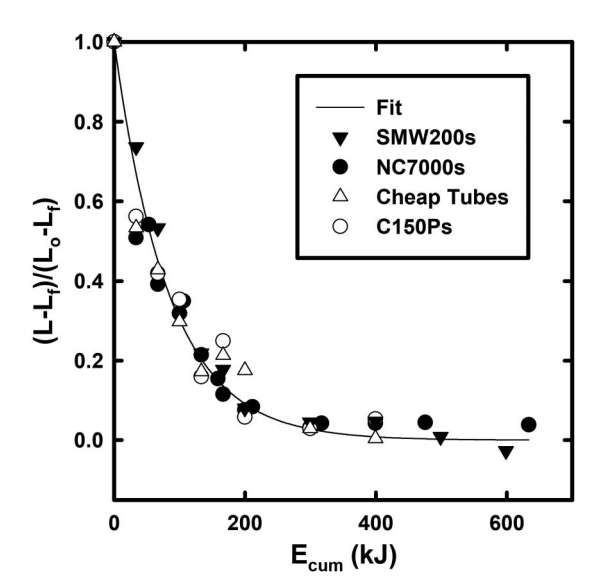


Figure 9. Cumulative energy data associated with the total impact energy collapsed to a single curve using the normalized length difference fit to the exponential given by Equation (12) with best fit E_{scale} value of 83.7 \pm 2.8 kJ with a standard error of regression of 0.0529.

reduction behaviors, and the exponential fit based on the cumulative energy of milling appears to describe the data well. While there is some clear discrepancy in the terminal behavior, the fitted terminal lengths fall within the experimental error of the measured terminal lengths. In fact, fitting the data from Figure 8 individually for each nanotube resulted in scaling energy values all within three standard deviations of the globally fitted scaling energy.

Instead of the length reduction being a function of the total impact energy used during milling, another possibility is that the minimum impact energy should be subtracted from the total impact energy for a single collision. Hence, we then define the effective impact energy, E_b^* , to be the difference between the total impact energy, E_b , and the minimum impact energy, $E_{b, \min}$, for a nanotube sample. The cumulative energy associated with the effective impact energy is then

$$E_{cum}^* = E_b^* v_t t = (E_b - E_{b, min}) v_t t$$
 (13)

Figure 10 is the normalized cumulative energy curve associated with the effective impact energy, and the scaling energy, E_{scale} , was found to be 59.3 ± 2.1 kJ. The goodness of fit to the effective cumulative energy is statistically similar to that of Figure 9. If the total impact energy is sufficiently large, then subtracting $E_{b, \min}$ from E_b will make no difference; Table 2 shows that $E_{b, \min}$ was significant compared to E_b except for Cheap Tubes. For Cheap Tubes, the minimum impact energy is considered to be zero, i.e. the effective impact energy is equal to the total impact energy. Consequently, the effective impact energy is noticeably greater for the Cheap Tubes than for the other three nanotube samples. Visual observation of Figure 10 shows the Cheap Tubes have slightly less agreement with the exponential model than the other three nanotube samples, especially at higher cumulative energies. To determine which model is more appropriate, impact energies closer to the minimum impact energy could be tested.

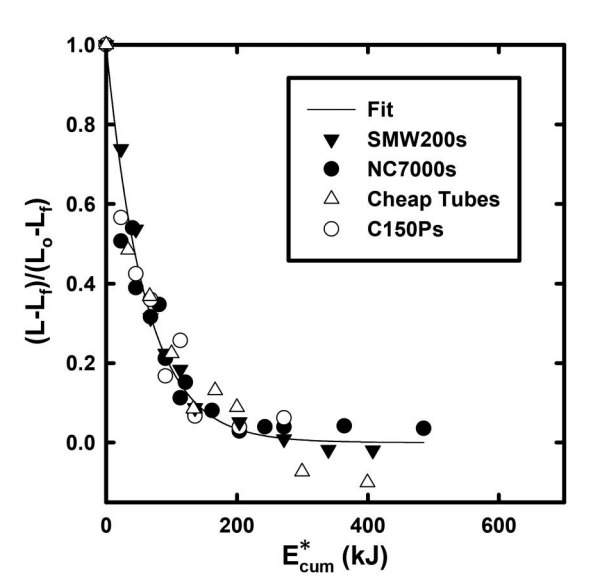


Figure 10. Cumulative energy data associated with the effective impact energy collapsed to a single curve using normalized length difference fit to the exponential given by Equation (12) with best fit E_{scale} value of 59.3 \pm 2.1 kJ with a standard error of regression of 0.0554.

Table 2. Impact energies associated with Figures 8 and 9 for the four commercial nanotubes.

MWCNT	E _b	E _{b, min}	E _b *
NC7000s	31 mJ	10 mJ	21 mJ
C150Ps	31 mJ	15 mJ	16 mJ
SMW200s	31 mJ	10 mJ	21 mJ
Cheap Tubes	31 mJ	< 3.5 mJ	31 mJ

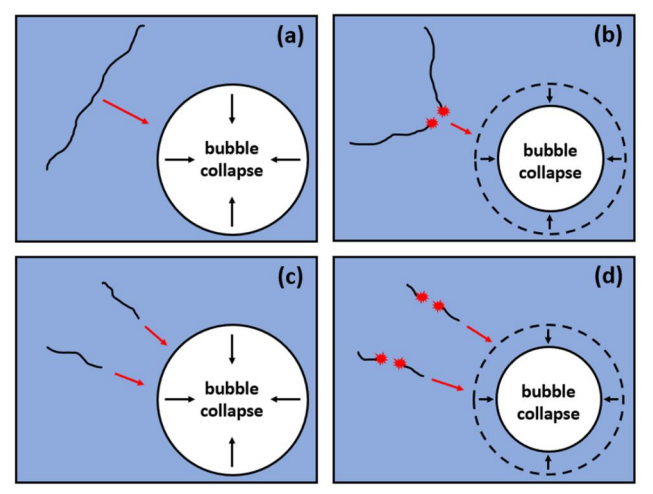


Figure 11. Sonication of carbon nanotubes imparts (a-b) radial buckling on long carbon nanotubes and (c-d) axial tension for short nanotubes. Red arrows indicate the force experienced by the nanotubes, and red dots indicate points of fracture

3.4. Comparison to length reduction by sonication

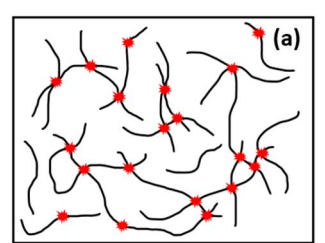
3.4.1. Mechanism of fracture

To our knowledge, sonication has been the only mode of carbon nanotube fracture other than milling in which the kinetics of length reduction have been studied. Initial studies on nanotube cleavage by sonication assumed a purely tensile mechanism by which the nanotubes orient radially as bubbles nucleate, grow, and collapse. The critical force, F_c , for nanotube breakage derived by Hennrich et al. and restated by Pagani et al. based on the tensile strength, σ_{break} , of the nanotube is given by the following

$$F_{c} = \sigma_{\text{break}} \pi \frac{(2Dw - w^{2})}{4} \tag{13}$$

where D is the diameter and w is the thickness of the wall. The discussions surrounding this equation involved only single-walled carbon nanotubes, and the critical force was estimated to be 20 nN. Later studies utilizing Brownian dynamics simulations found that long nanotubes can experience axial compression^[16] or align tangentially to bubbles and experience radial buckling. As the nanotubes shorten to approximately 1 μ m, the fracture mechanism can shift from buckling to tensile, which is shown in Figure 11.

Ball milling carbon nanotubes likely employs a purely buckling fracture mechanism. Because the carbon nanotube powder morphology consists of aggregates with randomly oriented and curved nanotubes, molecular dynamics simulations indicate that impact-induced fracture tends to occur at the intersections of adjacent nanotubes. [61] As illustrated in Figure 12, for very long nanotubes, there are initially many nanotube intersections at which impact induced fracture can



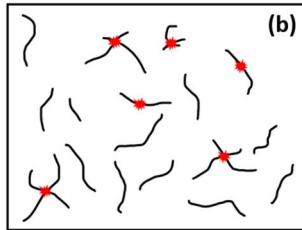


Figure 12. Representative schematic of impact induced fracture of (a) long and (b) short carbon nanotubes. Red dots indicate points of fracture. Most CNTs fracture points occur at CNT-CNT intersections, but isolated CNTs may fracture as well.

occur. As nanotubes shorten, the frequency of nanotube intersections decreases substantially consistent with exponential length reduction behavior with increasing cumulative impact energy.

Figure 13 shows characteristic capped and open nanotube tip morphologies as observed by HRTEM. Unmilled, parallel walled nanotubes appeared to have a relatively even distribution of capped and open ends as in Figure 13a,c, while the cup stacked Cheap Tubes had a much higher concentration of open ends. The narrow cone end of the cup stacked nanotubes occasionally had a capped tip as in Figure 13b, while the wide cone end was observed to always be open as in Figure 13d. Milled nanotubes that had been reduced to their terminal length contained a much higher concentration of open ends compared to unmilled nanotubes. Regardless of wall morphology, the most common end morphology of milled nanotubes involved a notable restriction in CNT diameter at the tip as in Figures 13e-f. This smaller diameter could be evidence of the proposed mechanism by which fracture occurs by buckling at nanotube intersections. It should be noted that observation of this end morphology in TEM is sensitive to the nanotube orientation relative to the electron beam. Also, caps on nanotube ends can reform after fracture due to being more configurationally favorable, so visual observation by TEM alone cannot validate the fracture mechanism. Capped nanotube ends present in milled samples could either be initially capped and undisturbed by milling or could be reformed after milling.

Many analogs exist between sonication of long nanotubes and ball milling. The increasing energy required for length reduction with increasing diameter appears to be consistent between the two processes. Also, both sonication and ball milling result in a terminal length, as experimental data from Lucas et al. showed length reduction convergence to an apparent terminal length at high cumulative ultrasonic energies. A potential difference between the two processes is the possibility of diameter reduction or complete wall stripping. While ball milling can induce defects on nanotube surfaces and ends, we and most others have found that carbon nanotube diameters remain constant during milling. However, wall stripping and slight diameter reduction has been reported for ultrasonication. [62]

3.4.2. Power law length reduction kinetics

Previous sonication studies used a power law to describe the kinetics of carbon nanotube length reduction. To compare

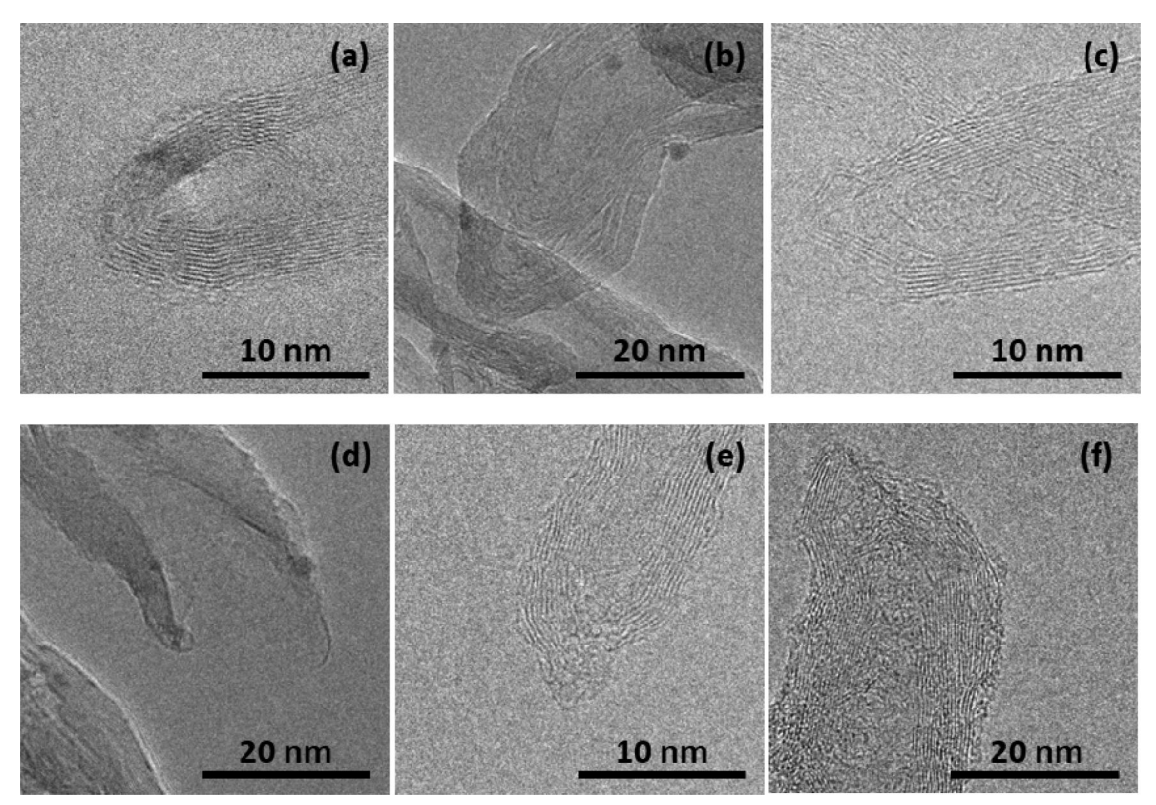


Figure 13. HRTEM micrographs of (a) capped NC7000s tip, (b) capped Cheap Tubes tip, (c) open NC7000s tip, (d) open Cheap Tubes tip, and (e-f) Constricted open tips.

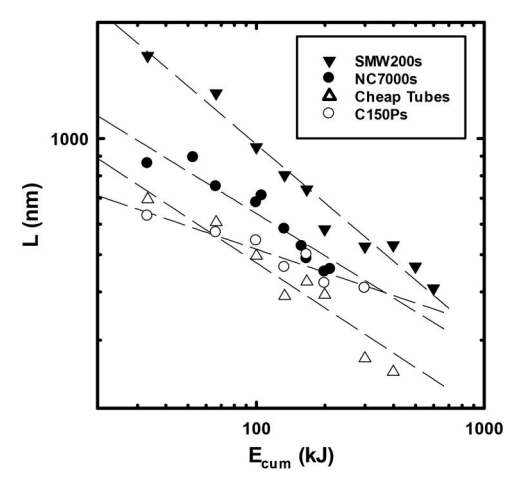


Figure 14. Length reduction of four commercial MWCNTs fit to a power law based on cumulative energy of milling. The kinetic behavior among the different carbon nanotubes varies significantly and appears to show higher rates of length reduction for nanotube samples with longer initial lengths.

our data with previous studies, a power law was fit to the length reduction data given in Figure 8. As was done previously, experimental data points at high cumulative energies that show a very small change in length reduction compared to points at lower energies were eliminated. The power law fit for the four commercial nanotube samples is shown in Figure 14.

The power law exponents that describe the length reduction kinetics of the nanotubes studied in this work are presented in Table 3 with comparisons to previous studies on sonication and ball milling. While the power law relationship in sonication studies was explicitly given, it was

necessary to extract ball milling data from graphs in milling studies (minimum of four data points) and fit the data to a power law to obtain the power law exponent. Figure S8 in the Supplementary Information shows these fits. To our knowledge, Table 3 encompasses all the kinetic length reduction data for sonication and milling in the current literature. The SMW200s power law exponent compares to the findings of Hennrich et al.^[14] and Jang et al.^[19] for sonication and Pierard et al.^[63] for ball milling, while the C150Ps power law exponent is akin to the findings of Lucas et al.[15] and other ball milling studies. [41,50,64]

Comparison among the four commercial nanotubes used in this study indicates the power law kinetics for length reduction by ball milling is dependent on the initial carbon nanotube length. The longest nanotube sample, SMW200s, exhibited the fastest rate of length reduction (e.g. highest power law exponent), and conversely, the shortest nanotube sample, C150Ps, exhibited the slowest rate of length reduction. This result is consistent with the trend found in previous ball milling studies, as Pierard et al. [63] used very long initial nanotubes, while the other ball milling studies used shorter initial nanotubes. [41,50,64] Sonication studies also exhibited a dependence on initial carbon nanotube length; however, the relationship is the inverse of that found for ball milling. Simulation results of Pagani et al.[17] suggested long and short nanotubes are described by power law exponents of roughly -0.22 and -0.5, respectively. The difference between the two processes could be explained by the difference in mechanism for different length nanotubes in sonication, whereas ball milling is assumed to have a consistent fracture mechanism independent of nanotube length.

Table 3. Power law relationships between cumulative energy of sonication/ball milling and carbon nanotube length.

Source		Power Law Relationship ^a
This Work (MWCNTs)	SMW200s	$L \propto E_{cum}^{-0.50}$
	NC7000s	$L \propto E_{cum}^{-0.36}$
	Cheap Tubes	$L \propto E_{cum}^{-0.39}$
	C150Ps	$L \propto E_{cum}^{-0.20}$
Hennrich et al. (SWCNTs)		$L \propto E_{US}^{-0.5}$
Lucas et al. (SWCNTs)	Graphistrength C100 (Arkema)	$L \propto E_{US}^{-0.21}; \ L \propto E_{US}^{-0.23}$
Jang et al. (MWCNTs)		$L \propto E_{US}^{-0.25}$
Pierard et al. (MWCNTs)		$L \propto E_{cum}^{-0.51}$
Kozma et al. (MWCNTs)		$L \propto E_{cum}^{-0.18}$
^b Papp et al. (MWCNTs)		$L \propto E_{cum}^{-0.20}$
^b Kukovecz et al. (MWCNTs)		$L \propto E_{cum}^{-0.20}$

^aBall milling studies are indicated by E_{cum} and sonication studies are indicated by E_{US} .

4. Conclusions

Length reduction of four commercial carbon nanotube samples was induced by planetary ball milling. The Burgio-Rojac model was used to calculate energy dissipated to the powder upon a single impact and cumulatively over the milling period. The minimum impact energy for carbon nanotube breakage appears to be a function of the diameter, but a sample with defects can eliminate the impact energy barrier. Defect density as measured by Raman spectroscopy could not be used to identify the minimum impact energy and was not correlated with nanotube length. The four commercial nanotubes were found to exhibit similar length reduction kinetics when collapsed to a master curve based on an exponential relation to the cumulative energy. Master curves governing the length reduction behavior for the four commercial nanotubes were developed using a total and effective impact energy with no statistically significant differences in fit quality, although the extent to which the total impact energy is above the minimum impact energy may play a role in the validity of this comparison. We believe the results of this study provide a good basis for describing the length reduction of any current commercially produced multiwalled carbon nanotubes, and also could prove essential to understanding the length reduction of very long carbon nanotubes.

Acknowledgements

We acknowledge Dr. Preston Larson and Dr. Julian Sabisch from the Samuel Roberts Noble Microscopy Lab for assistance with microscopy. We also acknowledge Dr. Megan Elwood-Madden for Raman spectroscopy training and equipment use.

Disclosure statement

No potential conflict of interest was reported by the author(s).

Funding

This research was supported by a grant from the National Science Foundation, [2022297], awarded through the CMMI program.

ORCID

Steven Crossley (b) http://orcid.org/0000-0002-1017-9839 Brian P. Grady (b) http://orcid.org/0000-0002-4975-8029

References

- [1] Liu, L.; Zhang, L.; Lua, J. Branched Carbon Nanotube Reinforcements for Improved Strength of Polyethylene Nanocomposites. *Appl. Phys. Lett.* **2012**, *101*, 161907. DOI: 10. 1063/1.4761936.
- [2] Rui, Y.; Guo, J. X.; Harwell, J.; Nakanishi, T.; Kotera, S.; Grady, B. P. Electrical, Mechanical, and Crystallization Properties of Ethylene-Tetrafluoroethylene Copolymer/Multiwalled Carbon Nanotube Composites. J. Appl. Polym. Sci. 2014, 131, 41052. DOI: 10.1002/app.41052.
- [3] Lin, B.; Sundararaj, U.; Potschke, P. Melt Mixing of Polycarbonate with Multi-Walled Carbon Nanotubes in Miniature Mixers. *Macromol. Mater. Eng.* 2006, 291, 227–238. DOI: 10.1002/mame.200500335.
- [4] Kasaliwal, G.; Goldel, A.; Potschke, P. Influence of Processing Conditions in Small-Scale Melt Mixing and Compression Molding on the Resistivity and Morphology of Polycarbonate-MWNT Composites. J. Appl. Polym. Sci. 2009, 112, 3494–3509. DOI: 10.1002/app.29930.
- [5] Socher, R.; Krause, B.; Muller, M. T.; Boldt, R.; Potschke, P. The Influence of Matrix Viscosity on MWCNT Dispersion and Electrical Properties in Different Thermoplastic Nanocomposites. *Polymer* 2012, 53, 495–504. DOI: 10.1016/j.polymer.2011.12.019.
- [6] Guo, J. X.; Liu, Y. J.; Prada-Silvy, R.; Tan, Y. Q.; Azad, S.; Krause, B.; Potschke, P.; Grady, B. P. Aspect Ratio Effects of Multi-Walled Carbon Nanotubes on Electrical, Mechanical, and Thermal Properties of Polycarbonate/MWCNT Composites. J. Polym. Sci. 2014, 52, 73–83. DOI: 10.1002/polb.23402.
- [7] Hong, W. T.; Tai, N. H. Investigations on the Thermal Conductivity of Composites Reinforced with Carbon Nanotubes. *Diam. Relat. Mater.* 2008, 17, 1577–1581. DOI: 10. 1016/j.diamond.2008.03.037.
- [8] Krause, B.; Barbier, C.; Kunz, K.; Potschke, P. Comparative Study of Singlewalled, Multiwalled, and Branched Carbon Nanotubes Melt Mixed in Different Thermoplastic Matrices. *Polymer* 2018, 159, 75–85. DOI: 10.1016/j.polymer.2018.11.010.
- [9] Castillo, F. Y.; Socher, R.; Krause, B.; Headrick, R.; Grady, B. R.; Prada-Silvy, R.; Potschke, P. Electrical, Mechanical, and Glass Transition Behavior of Polycarbonate-Based Nanocomposites with Different Multi-Walled Carbon Nanotubes. *Polymer* 2011, 52, 3835–3845. DOI: 10.1016/j.polymer.2011.06.018.
- [10] Sandler, J.; Shaffer, M. S. P.; Prasse, T.; Bauhofer, W.; Schulte, K.; Windle, A. H. Development of a Dispersion Process for Carbon Nanotubes in an Epoxy Matrix and the Resulting

^bA poor power law fit ($R^2 < 0.9$) was found for the data in these studies as shown in Figure S5.

- Electrical Properties. Polymer 1999, 40, 5967-5971. DOI: 10. 1016/s0032-3861(99)00166-4.
- [11] Menzer, K.; Krause, B.; Boldt, R.; Kretzschmar, B.; Weidisch, R.; Potschke, P. Percolation Behaviour of Multiwalled Carbon Nanotubes of Altered Length and Primary Agglomerate Morphology in Melt Mixed Isotactic Polypropylene-Based Composites. Compos. Sci. Technol. 2011, 71, 1936-1943. DOI: 10.1016/j.compscitech.2011.09.009.
- Tinh, T. X.; Chuc, N. V.; Jourdain, V.; Paillet, M.; Kim, D. Y.; [12] Sauvajol, J. L.; Ngo, T. T. T.; Minh, P. N. Synthesis of Individual Ultra-Long Carbon Nanotubes and Transfer to Other Substrates. J. Exp. Nanosci. 2011, 6, 547-556. DOI: 10. 1080/17458080.2010.498839.
- Briggs, N. M.; Crossley, S. P. Rapid Growth of Vertically Aligned Multi-Walled Carbon Nanotubes on a Lamellar Support. RSC Adv. 2015, 5, 83945-83952. DOI: 10.1039/ C5RA12611H.
- Hennrich, F.; Krupke, R.; Arnold, K.; Stutz, J. A. R.; Lebedkin, S.; Koch, T.; Schimmel, T.; Kappes, M. M. The Mechanism of Cavitation-Induced Scission of Single-Walled Carbon Nanotubes. J. Phys. Chem. B 2007, 111, 1932-1937. DOI: 10. 1021/jp065262n.
- [15] Lucas, A.; Zakri, C.; Maugey, M.; Pasquali, M.; van der Schoot, P.; Poulin, P. Kinetics of Nanotube and Microfiber Scission under Sonication. J. Phys. Chem. C 2009, 113, 20599-20605. DOI: 10.1021/jp906296y.
- [16] Chew, H. B.; Moon, M. W.; Lee, K. R.; Kim, K. S. Compressive Dynamic Scission of Carbon Nanotubes under Sonication: Fracture by Atomic Ejection. Proc. R Soc. A 2011, 467, 1270-1289. DOI: 10.1098/rspa.2010.0495.
- [17] Pagani, G.; Green, M. J.; Poulin, P.; Pasquali, M. Competing Mechanisms and Scaling Laws for Carbon Nanotube Scission by Ultrasonication. Proc. Natl. Acad. Sci. U S A 2012, 109, 11599-11604. DOI: 10.1073/pnas.1200013109.
- Liu, P.; Wang, T. M. Ultrasonic-Assisted Chemical Oxidative Cutting of Multiwalled Carbon Nanotubes with Ammonium Persulfate in Neutral Media. Appl. Phys. A 2009, 97, 771-775. DOI: 10.1007/s00339-009-5314-z.
- Jang, J. W.; Lee, C. E.; Lee, C. J. Exponential Decrease of Scission Length and Low Tensile Strength of Bamboo-Shaped Multi-Walled Carbon Nanotubes under Ultrasonication. Curr. Appl. Phys. 2017, 17, 507-512. DOI: 10.1016/j.cap.2017.01.012.
- Zhang, D. S.; Shi, L. Y.; Fang, J. H.; Li, X. K.; Dai, K. Preparation and Modification of Carbon Nanotubes. Mater. Lett. 2005, 59, 4044-4047. DOI: 10.1016/j.matlet.2005.07.081.
- Konya, Z.; Vesselenyi, I.; Niesz, K.; Kukovecz, A.; Demortier, A.; Fonseca, A.; Delhalle, J.; Mekhalif, Z.; Nagy, J. B.; Koos, A. A.; et al. Large Scale Production of Short Functionalized Carbon Nanotubes. Chem. Phys. Lett. 2002, 360, 429-435. DOI: 10.1016/s0009-2614(02)00900-4.
- [22] Rubio, N.; Fabbro, C.; Herrero, M. A.; de la Hoz, A.; Meneghetti, M.; Fierro, J. L. G.; Prato, M.; Vazquez, E. Ball-Milling Modification of Single-Walled Carbon Nanotubes: Purification, Cutting, and Functionalization. Small 2011, 7, 665-674. DOI: 10.1002/smll.201001917.
- Ma, P. C.; Wang, S. Q.; Kim, J. K.; Tang, B. Z. In-Situ Amino Functionalization of Carbon Nanotubes Using Ball Milling. J. Nanosci. Nanotechnol. 2009, 9, 749-753. DOI: 10.1166/jnn. 2009.C017.
- Javadi, A.; Mirdamadi, S.; Faghihisani, M.; Shakhesi, S.; Soltani, R. Well-Dispersion of Multi-Walled Carbon Nanotubes in Aluminum Matrix Composites by Controlling the Mixing Process. Fuller. Nanotub. Carbon Nanostructures 2013, 21, 436-447. DOI: 10.1080/1536383X.2011.629758.
- [25] Qi, H. X.; Zhao, B. Influence of Multi-Walled Carbon Nanotube Addition on the Properties of Sn. Fuller. Nanotub. Carbon Nanostructures 2015, 23, 406-409. DOI: 10.1080/ 1536383X.2013.833913.
- Evlen, H.; Akcaer, E. Effects of Wear Load on Mechanical and [26] Morphological Properties of A356 Matrix Carbon Nano Tube

- Composites. Fuller. Nanotub. Carbon Nanostructures 2019, 27, 351-357. DOI: 10.1080/1536383X.2019.1575817.
- [27] Naoui, Y.; Settar, A.; Chetehouna, K.; Bouleklab, M. C.; Revo, S.; Hamamda, S. Effect of Multiwall Carbon Nanotube (MWCNT) Content on Thermal and Structural Properties Enhancement of FeCu-MWCNT Nanocomposites Synthesized by High-Energy Ball Milling. Appl. Phys. A 2020, 126, 283. DOI: 10.1007/s00339-020-03474-w.
- Farbod, M.; Norouzi, E. Microstructure, Mechanical and Electrical Properties of Al/Carbon Nanotubes Composite. Fuller. Nanotub. Carbon Nanostruct. 2022, 30, 603-606. DOI: 10.1080/1536383X.2021.1986016.
- Cao, L.; Chen, B.; Wan, J.; Shen, J. H.; Li, J. S. Improving Carbon Nanotube Dispersion in Aluminum Matrix Composite Powders by a Repeating-Deformation Ball Milling Process. Mater. Charact. 2023, 201, 112986. DOI: 10.1016/j.matchar. 2023.112986.
- Cao, L.; Chen, B.; Wan, J.; Shen, J. H.; Li, S. F.; Liu, S. Q.; Li, J. S. Unraveling the Dispersion Mechanism of Carbon Nanotubes in Aluminum Powder Particles during High Energy Ball Milling by FIB-TEM Study. Powder Technol. 2023, 419, 118339. DOI: 10.1016/j.powtec.2023.118339.
- Guler, O.; Guler, S. H.; Yo, F.; Aydin, H.; Aydin, C.; El-Tantawy, F.; Duraia, E. M.; Fouda, A. N. Electrical and Optical Properties of Carbon Nanotube Hybrid Zinc Oxide Nanocomposites Prepared by Ball Mill Technique. Fuller. Nanotub. Carbon Nanostruct. 2015, 23, 865-869. DOI: 10.1080/ 1536383X.2015.1022256.
- Major, J.; Seo, J. W.; Horvath, E.; Kukovecz, A.; Forro, L.; Hernadi, K. Electron Microscopy Investigation of Coated Multiwall Carbon Nanotubes Prepared by Reactive Ball Milling. J. Nanosci. Nanotechnol. 2019, 19, 502-508. DOI: 10.1166/jnn. 2019.15775.
- Pham, V. V.; Dang, H. Q.; Nguyen, T. T.; Cao, T. M. A Facile Ball-Milling Method to Combine Carbon Nanotubes and Commercial TiO2 towards Nitrogen Oxide Photocatalytic Removal. J. Aust. Ceram. Soc. 2023. DOI: 10.1007/s41779-023-00890-y.
- Benigno, E.; Lorente, M. A.; Olmos, D.; Gonzalez-Gaitano, G.; Gonzalez-Benito, J. Nanocomposites Based on Low Density Polyethylene Filled with Carbon Nanotubes Prepared by High Energy Ball Milling and Their Potential Antibacterial Activity. Polym. Int. 2019, 68, 1155-1163. DOI: 10.1002/pi.5808.
- Jiang, J. J.; Shu, Y.; Xu, L.; Li, W. P.; Zhang, H.; Liu, W. J.; Long, X. L.; Zhou, C. L.; Wang, L.; Qu, M. Z. Preparation of High-Yield Multi-Walled Carbon Nanotubes by Catalytic Decomposition of Mixture of Natural Gas and Propylene and Their Electrothermal Properties. Fuller. Nanotub. Carbon Nanostructures 2020, 28, 745-751. DOI: 10.1080/1536383X. 2020.1758674.
- Pei, X. Y.; Zhao, M. Y.; Li, R. X.; Lu, H.; Yu, R. R.; Xu, Z. W.; Li, D. S.; Tang, Y. H.; Xing, W. J. Porous Network Carbon Nanotubes/Chitosan 3D Printed Composites Based on Ball Milling for Electromagnetic Shielding. Compos. A Appl. Sci. Manuf. 2021, 145, 106363. DOI: 10.1016/j.compositesa.2021. 106363.
- [37] Gao, Z. Q.; Han, Q. J. B.; Liu, J. B.; Zhao, K. B.; Yu, Y.; Feng, Y. Y.; Han, S. S. Dispersion of Carbon Nanotubes Improved by Ball Milling to Prepare Functional Epoxy Nanocomposites. Coatings 2023, 13, 649. DOI: 10.3390/coatings13030649.
- Liu, F.; Zhang, X. B.; Cheng, J. P.; Tu, J. P.; Kong, F. Z.; Huang, W. Z.; Chen, C. P. Preparation of Short Carbon Nanotubes by Mechanical Ball Milling and Their Hydrogen Adsorption Behavior. Carbon 2003, 41, 2527-2532. DOI: 10. 1016/s0008-6223(03)00302-6.
- Pierard, N.; Fonseca, A.; Colomer, J. F.; Bossuot, C.; Benoit, J. M.; Van Tendeloo, G.; Pirard, J. P.; Nagy, J. B. Ball Milling Effect on the Structure of Single-Wall Carbon Nanotubes. Carbon 2004, 42, 1691-1697. DOI: 10.1016/j.carbon.2004.02.

- Elbadawi, N. A.; Ramadan, A. R.; Esawi, A. M. K. Studying the Effect of Shortening Carbon Nanotubes via Ball Milling on Cellulose Acetate Nanocomposite Membranes for Desalination Applications. Membranes 2022, 12, 474. DOI: 10.3390/ membranes12050474.
- [41] Kukovecz, A.; Kanyo, T.; Konya, Z.; Kiricsi, I. Long-Time Low-Impact Ball Milling of Multi-Wall Carbon Nanotubes. Carbon 2005, 43, 994-1000. DOI: 10.1016/j.carbon.2004.11.030.
- Burgio, N.; Iasonna, A.; Magini, M.; Padella, F. Mechanical Alloying of the Fe-Zr System in Different Milling Condition. J. Phys. 1990, 51, C4265-C4271.
- [43] Burgio, N.; Iasonna, A.; Magini, M.; Martelli, S.; Padella, F. Mechanical Alloying of the Fe-Zr system - Correlation between Input Energy and End-Products. Nuovo. Cimento. Dell. 1991, 13, 459-476. DOI: 10.1007/BF02452130.
- Iasonna, A.; Magini, M. Power Measurements during Mechanical Milling. An Experimental Way to Investigate the Energy Transfer Phenomena. Acta Mater. 1996, 44, 1109-1117. DOI: 10.1016/1359-6454(95)00226-x.
- Magini, M.; Iasonna, A.; Padella, F. Ball Milling: An Experimental Support to the Energy Transfer Evaluated by the Collision Model. Scr. Mater. 1996, 34, 13-19. DOI: 10.1016/ 1359-6462(95)00465-3.
- Magini, M.; Iasonna, A. Energy-Transfer in Mechanical [46] Alloying. Mater. Trans. JIM 1995, 36, 123-133. DOI: 10.2320/ matertrans1989.36.123.
- [47] Padella, F.; Paradiso, E.; Burgio, N.; Magini, M.; Martelli, S.; Guo, W.; Iasonna, A. Mechanical Alloying of the Pd-Si System in Controlled Conditions of Energy-Transfer. J. Less-Common Met. 1991, 175, 79-90. DOI: 10.1016/0022-5088(91)90351-4.
- Guo, W.; Iasonna, A.; Magini, M.; Martelli, S.; Padella, F. Synthesis of Amorphous and Metastable Ti40Al60 Alloys by Mechanical Alloying of Elemental Powders. J. Mater. Sci. 1994, 29, 2436-2444. DOI: 10.1007/BF00363438.
- Liu, L.; Magini, M. Correlation between Energy Transfers and Solid State Reactions Induced by Mechanical Alloying on the Mo33Si66 System. J. Mater. Res. 1997, 12, 2281-2287. DOI: 10. 1557/JMR.1997.0304.
- Kozma, G.; Puskas, R.; Papp, I. Z.; Belteky, P.; Konya, Z.; [50] Kukovecz, A. Experimental Validation of the Burgio-Rojac Model of Planetary Ball Milling by the Length Control of Multiwall Carbon Nanotubes. Carbon 2016, 105, 615-621. DOI: 10.1016/j.carbon.2016.05.005.
- [51] Zapata, H. J. A.; Crossley, S.; Grady, B. P. Influence of Tapped Density on the Degradation Profile of Multiwall Carbon Nanotubes. Thermochim. Acta 2017, 654, 140-145. DOI: 10. 1016/j.tca.2017.05.014.
- [52] Krause, B.; Boldt, R.; Pötschke, P. A Method for Determination of Length Distributions of Multiwalled Carbon Nanotubes

- before and after Melt Processing. Carbon 2011, 49, 1243-1247. DOI: 10.1016/j.carbon.2010.11.042.
- [53] Xie, S. S.; Li, W. Z.; Pan, Z. W.; Chang, B. H.; Sun, L. F. Carbon Nanotube Arrays. Mater. Sci. Eng. A-2000, 286, 11-15. DOI: 10.1016/s0921-5093(00)00657-2.
- [54] Dresselhaus, M. S.; Dresselhaus, G.; Saito, R.; Jorio, A. Raman Spectroscopy of Carbon Nanotubes. Phys. Rep. 2005, 409, 47-99. DOI: 10.1016/j.physrep.2004.10.006.
- Smart, S. K.; Ren, W. C.; Cheng, H. M.; Lu, G. Q.; Martin, D. J. Shortened Double-Walled Carbon Nanotubes by High-Energy Ball Milling. IJNT. 2007, 4, 618-633. DOI: 10.1504/IJNT.2007.
- Forro, L.; Gaal, R.; Grimaldi, C.; Mionic, M.; Ribic, P. R.; [56] Smajda, R.; Magrez, A. Tuning the Length Dispersion of Multi-Walled Carbon Nanotubes by Ball Milling. Aip Advances 2013, 3, 092117. DOI: 10.1063/1.4821802.
- Guo, J. X.; Briggs, N.; Crossley, S.; Grady, B. P. A New Finding for Carbon Nanotubes in Polymer Blends: Reduction of Nanotube Breakage during Melt Mixing. J. Thermoplast. Compos. Mater. 2018, 31, 110-118. DOI: 10.1177/0892705716681835.
- Rojac, T.; Kosec, A.; Malic, B.; Holc, J. The Application of a Milling Map in the Mechanochemical Synthesis of Ceramic Oxides. J. Eur. Ceram. Soc. 2006, 26, 3711-3716. DOI: 10.1016/ j.jeurceramsoc.2005.11.013.
- [59] Li, Y. B.; Wei, B. Q.; Liang, J.; Yu, Q.; Wu, D. H. Transformation of Carbon Nanotubes to Nanoparticles by Ball Milling Process. Carbon 1999, 37, 493-497. DOI: 10.1016/ s0008-6223(98)00218-8.
- Kim, Y. A.; Hayashi, T.; Fukai, Y.; Endo, M.; Yanagisawa, T.; Dresselhaus, M. S. Effect of Ball Milling on Morphology of Cup-Stacked Carbon Nanotubes. Chem. Phys. Lett. 2002, 355, 279-284. DOI: 10.1016/s0009-2614(02)00248-8.
- Ozden, S.; Machado, L. D.; Tiwary, C.; Autreto, P. A. S.; Vajtai, [61] R.; Barrera, E. V.; Galvao, D. S.; Ajayan, P. M. Ballistic Fracturing of Carbon Nanotubes. ACS Appl. Mater. Interfaces. 2016, 8, 24819-24825. DOI: 10.1021/acsami.6b07547.
- [62] Lu, K. L.; Lago, R. M.; Chen, Y. K.; Green, M. L. H.; Harris, P. J. F.; Tsang, S. C. Mechanical Damage of Carbon Nanotubes by Ultrasound. Carbon 1996, 34, 814-816. DOI: 10.1016/0008-6223(96)89470-x.
- Pierard, N.; Fonseca, A.; Konya, Z.; Willems, I.; Van Tendeloo, G.; Nagy, J. B. Production of Short Carbon Nanotubes with Open Tips by Ball Milling. Chem. Phys. Lett. 2001, 335, 1-8. DOI: 10.1016/s0009-2614(01)00004-5.
- Papp, I. Z.; Kozma, G.; Puskas, R.; Simon, T.; Konya, Z.; Kukovecz, A. Effect of Planetary Ball Milling Process Parameters on the Nitrogen Adsorption Properties of Multiwall Carbon Nanotubes. Adsorption 2013, 19, 687-694. DOI: 10. 1007/s10450-013-9493-8.